EPJ Photovoltaics **2**, 20401 (2011)
www.epj-pv.org
DOI: 10.1051/epjpv/2011021

Electrodeposition of nanoporous ZnO on Al-doped ZnO leading to a highly organized structure for integration in Dye Sensitized Solar Cells

S. Haller[a], J. Rousset, G. Renou, and D. Lincot

Institute of Research and Development of Photovoltaic Energy (IRDEP) -UMR 7174-EDF-CNRS-Chimie ParisTech, 6 quai Watier, 78401 Chatou Cedex, France

Received: 10 January 2011 / Accepted: 13 July 2011
Published online: 10 October 2011

Abstract In the present study, we propose an improvement of the anode configuration in Zinc Oxide based Dye Sensitized Solar Cells (DSSC). Instead of the classical configuration, which is composed by two different metal oxides: one transparent conducting oxide (TCO) for the substrate and one nanostructured metal oxide for supporting the dye, the new approach is to use ZnO as unique material. Thus, nanoporous zinc oxide films have been electrodeposited on a sputtered Al doped ZnO layers with varying thicknesses up to 6 μm. The evolution of the porosity of the structure has been studied by scanning electron microscope (SEM) and electrochemical impedance spectroscopy and compared with standard nanoporous ZnO grown on fluorine doped tin oxide (SnO_2:F noted FTO).
This results firstly in the modification of the nanoporous structure morphology and secondly a better adhesion between the nanoporous layer and the substrate. Organization in the nanoporous material is enhanced with regular pores arrays and perpendicular to the substrate. Dye sensitized solar cells based on this simplified architecture present efficiencies up to 4.2% and 4.5% with N719 and D149 respectively as sensitizers. Higher fill factor and Voc are found in comparison with the one obtained for deposition on the classical transparent conducting oxide (FTO), which denote improved electrical transfer properties.

1 Introduction

Dye sensitized solar cells (DSSC) are recognized as a credible option among photovoltaic technologies [1,2]. Although efficiencies up to 11% have been achieved with TiO_2 based anodes, zinc oxide is considered as a promising alternative material. While both materials present similar band gap energies (3.4 eV for ZnO [3] and 3.2 eV for TiO_2 [4] at room temperature), the electrical properties of ZnO are far superior [5], especially in terms of electron mobility [6] (115−155 $cm^2\ V^{-1}\ s^{-1}$ for ZnO vs. 30 $cm^2\ V^{-1}\ s^{-1}$ for TiO_2). Moreover, ZnO is a more reactive material, and enables deposition under various mild conditions. Indeed this material can be deposited with low temperature and non-vacuum methods such as chemical bath deposition [7] (CBD), hydrothermal method [8, 9], metal vapor transport oxidation method [10], spray deposition [11] and electrodeposition [12,13] (ED).

We will focus more particularly in this paper on the electrodeposition technique that is a low cost method suitable for large-scale production and deposition on flexible substrate because of the low temperatures involved. Since the pioneering works of Peulon et al. [12] and Izaki et al. [13] published in 1996, and thanks to the large number of studies carried out on this topic, the growth of ZnO by electrodeposition is now well described. Indeed a large variety of geometries can be achieved by this method by modifying the bath composition, such as dense or nanoporous layers (np) [14], nanowires [15] or nanotubes [16]... and many of them have been tested as anode in DSSC [17–21]. Among other properties such as transparency or good electron mobility, the material involved in the anode fabrication has to present a large developed surface, in order to maximize the absorption of the incident light by the dye. ZnO nanoporous films prepared by co-deposition with dye molecules particularly meet these specifications [22]. Thus efficiencies up to 5.6% have been reached with a nanoporous structure obtaiend with Eosin Y (EY) as structure directing agent and with D149 as a sensitizer [23] and an efficiency of 4.6% is recorded elsewhere in the same conditions [24].

Nanoporous ZnO has been deposited on transparent conductive oxide (TCO), GaN [25] and metals [26]. Classically, TCO such as fluorine tin oxide (FTO) and indium tin oxide (ITO) are preferred since it allows a front side illumination. Both are creating heterojunctions with electrodeposited nanoporous ZnO resulting into structural and chemical mismatches, which can limit the electrical transfer. Homojunction has been performed but only in

[a] e-mail: Servane-Haller@etu.chimie-paristech.fr

the case of deposition of a buffer layer of ZnO by CVD on GaN prior electrodeposition of nanoporous ZnO [27]. In the present study, we explore the possibility to use directly ZnO deposited by sputtering on glass as substrate, which could promote optimal interfacial properties thanks to a homoepitaxial growth and keep interesting optical properties. In addition, ZnO is more and more substituting those classical oxides as TCO, especially indium doped tin oxide and fluorine doped tin oxide because it has the advantage over the first one that all of its components are abundant and on the second one that it is possible to deposit it on plastic foils.

In this work, we have deposited nanoporous ZnO on sputtered ZnO:Al and studied the influence of the substrate on the morphology and on cell performances in comparison with structures deposited on FTO glass.

Optimization has been carried out on this bilayer structure (sputtered Al:ZnO/nanoporous ZnO) and on the coloration conditions for two key-dyes: a ruthenium based dye (N719) [28] and an organic dye (D149) [29]. The first one is well-known for its good performances on TiO_2 [30] and the second one is reported as promising for ZnO-based solar cells [31,32]. Efficiencies up to 4.2% and 4.5% were achieved with N719 and D149 as sensitizers respectively.

2 Experimental section

Preparation of FTO glass: fluorine doped SnO_2 (FTO) coated glasses (10 Ω/cm^2) Asahi glass sheets were cleaned ultrasonically in water, acetone and ethanol. They were activated in 45% HNO_3 for 2 min and finally rinsed with distilled water prior the electrodeposition.

Preparation of Al:ZnO substrate: a 800 nm thick ZnO:Al is deposited by RF sputtering with a sheet resistance of 10 Ω/cm^2 with a preferential (001) orientation. Its carrier density was measured to be 4×10^{20} cm^{-3} with a mobility of $\mu = 15$ cm^2 V^{-1} s^{-1}.

Deposition of the nanoporous ZnO: the electrolyte (Milli-Q pure water 18.2 MΩ) is composed of 5 mM $ZnCl_2$ (VWR), 0.1 M KCl (VWR) using and 50 μM sodium salt of EY (Sigma Aldrich) as structure directing agent. A classical three-electrode set-up was used with a Pt wire as a counter electrode. The potential of –1.4 V was referred to a mercury sulfate electrode (MSE) reference electrode (+0.65 V vs. NHE). The cell was placed in a thermostated bath maintained at 75 °C. Oxygen gas was bubbled at 100 mL/min for 1 hour prior the actual electrolysis and the same gas flow was maintained during the deposition.

Deposition of a buffer layer: for some experiments on FTO glass, dense ZnO was deposited prior deposition of nanoporous ZnO. The electrolyte is the same as the one for electrodeposition on nanoporous structure, but without Eosin Y. The same set-up and the same conditions were used. Deposition of 0.7 C/cm^2 of dense ZnO was performed, corresponding to a thickness of 400 nm.

Film Characterization: film thickness was measured with a Dektak 6M Stylus Profiler. Morphology was studied by scanning electron microscope (SEM) (Leika S440). Optical properties of the materials were investigated by optical transmission with a Perkin Elmer Lambda 900 spectrometer. Porosity was calculated considering the film thickness and the amount of ZnO deposited measured by X-Ray fluorescence spectrometry (Fisherscope X-Ray XAN). Surface area of the films is deduced from impedance measurements as described in Dupuy et al. [33]. Roughness factor is given as the ratio of the measured surface area on the projected film area.

Cell preparation: desorption of the as-prepared film is carried out in a KOH solution (pH 10.5) for 24 h. Readsorption of N719 (Dyesol) and D149 (Mitsubishi Paper Mills) were carried out in 0.5 mM dye in ethanolic solution and in 0.5 mM dye in ter-butyl alcohol/acetonitrile (1/1) respectively. The electrolyte is a methoxypropionitrile dissolving 0.5 M tetrabutylammonium iodide and 0.05 M I_2 as redox electrolyte (Solaronix). Counter electrode is thermally platinized FTO glass (with Platisol from Solaronix, heated at 450 °C for 15 min).

Cell characterizations: photocurrent density was measured under illumination with AM 1.5 simulated sun light (100 mW/cm^2) on a 0.125 cm^2 surface delimited with an absorbing material. A Spectra-Nova technologies solar simulator system was used for these measurements. Cells were illuminated through the photo-anode.

3 Results and discussion

3.1 Structural properties

Three different cases have been investigated, whether the growth of the nanoporous structure was performed on the FTO substrate, directly or on a compact ZnO buffer layer preliminary electrodeposited (ZnO:ED), or on a sputtered ZnO:Al on glass.

The morphologies of the nanoporous layers grown on the different substrates are presented in Figure 1. With the FTO glass substrate (with or without ZnO:ED) (Figs. 1a and 1b), the organization of the electrodeposited ZnO film corresponds to that described in literature [34]. The views of the cross section show tilted pores of various orientations and reveal a surface roughness on the top of the structure. Nanoporous ZnO units are identifiable thanks to the pore orientations and to the round shaped relief on the sample surface. These well-defined units have been shown to be single-crystalline [34].

Cross-section SEM images of films deposited on ZnO:Al show regular pores perpendicular to the substrate (Fig. 1c). No relief can be observed on top views and no nanoporous ZnO unit could therefore be identified. Thus, the organization of the structure is considerably enhanced in comparison with structure of nanoporous ZnO deposited on FTO glass.

Above a certain thickness, a peeling off of the layer occurs. The less stable layers are the ones deposited directly on FTO glass. A slight enhancement of the mechanical stability is obtained when a dense ZnO layer is electrodeposited prior to the electrodeposition of the nanoporous

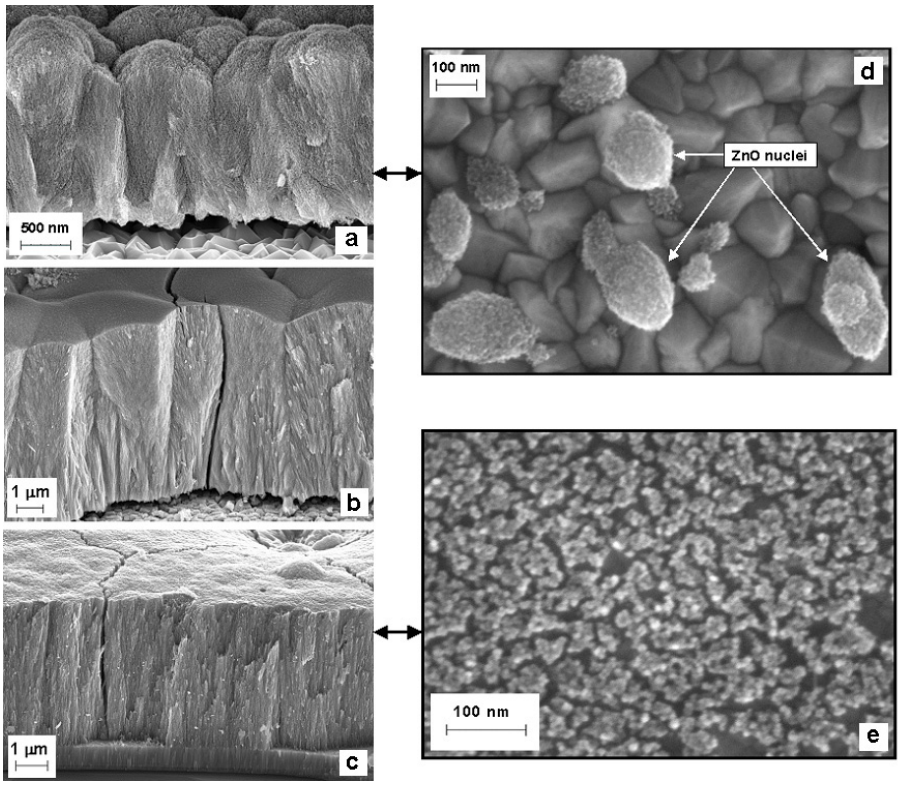

Fig. 1. SEM images of ZnO mesoporous structure deposited on (a) FTO glass, (b) a 400 nm thick bulk ZnO buffer layer deposited on FTO glass and (c) sputtered Al:ZnO. Deposition of the nanoporous structure on (d) FTO glass and (e) Al:ZnO respectively after deposition of 0.01 C/cm^2.

layer. However, the enhancement of adhesion to the substrate is more obvious when deposition is performed on ZnO:Al.

In order to go further into the growth mechanism understanding, SEM images have been carried out in the first steps of the synthesis. After 0.01 C/cm^2 (10s) of electrodeposition isolated nuclei are observed on the FTO surface, characteristic of a three-dimensional growth mechanism as shown in the Figure 1. On the contrary in the case of the growth on ZnO:Al and for the same amount of consumed charge, the substrate surface is almost homogenously covered by the ZnO nuclei suggesting a much easier nucleation process (Fig. 1e). This would correspond to the fact that no nucleation barrier is expected for the homoepitaxial growth of ZnO on ZnO, as observed in previous works [19,35]. Moreover, measurements presented in these works show the c-axis of the electrodeposited ZnO to be continuous to the one of the ZnO substrate.

Figure 2 shows the X-Ray diffraction (XRD) pattern performed on ZnO:Al substrate, nanoporous ZnO deposited on ZnO:Al and on SnO_2:F. On each diffractogram, the peak corresponding to the diffraction of the incident beam on the {002} plans can be seen, showing that the layer is highly oriented along the c-axis of the wurtzite structure perpendicularly to the substrate surface. The position of this peak varies depending on the substrate. For deposition on FTO glass, (002) peak is observed at the relaxed position (34.42°according to the ICDD pattern 00-036-1451), implying a growth without stress, which is consistent with the 3D nucleation observed on SEM images. Moreover, the diffractogram of the nanoporous ZnO deposited on FTO glass shows other peaks apart from the (002) peak of ZnO. Some are due to the SnO_2 pattern but the (100), (101), (102) and (103) peaks of the wurtzite structure also appear, showing that the preferential orientation of the ZnO is less pronounced on FTO glass. On the diffractogram of the ZnO:Al substrate, the diffraction of the incident beam on the {002} plans appears at 34.27°, which is slightly shifted from the expected position (34.42°) due to the compressive stress in the layer. In the case of electrodeposition of nanoporous ZnO on ZnO:Al substrate, the angular position of the peak (002) is 34.34°, which is a mean value between that of stressed sputtered ZnO:Al and that of electrodeposited ZnO on FTO. Further experiments are needed to determine the origin of the peak position evolution but the conservation of the stress of the substrate during the first stages of growth of the electrodeposited ZnO could be an explanation of this phenomenon.

3.2 Optical properties

Optical characterizations have been performed on the layer obtained on electrodeposited ZnO/FTO glass and ZnO:Al glass (Fig. 3). In any case the structure substrate/nanoporous ZnO transmits close to 80% of the

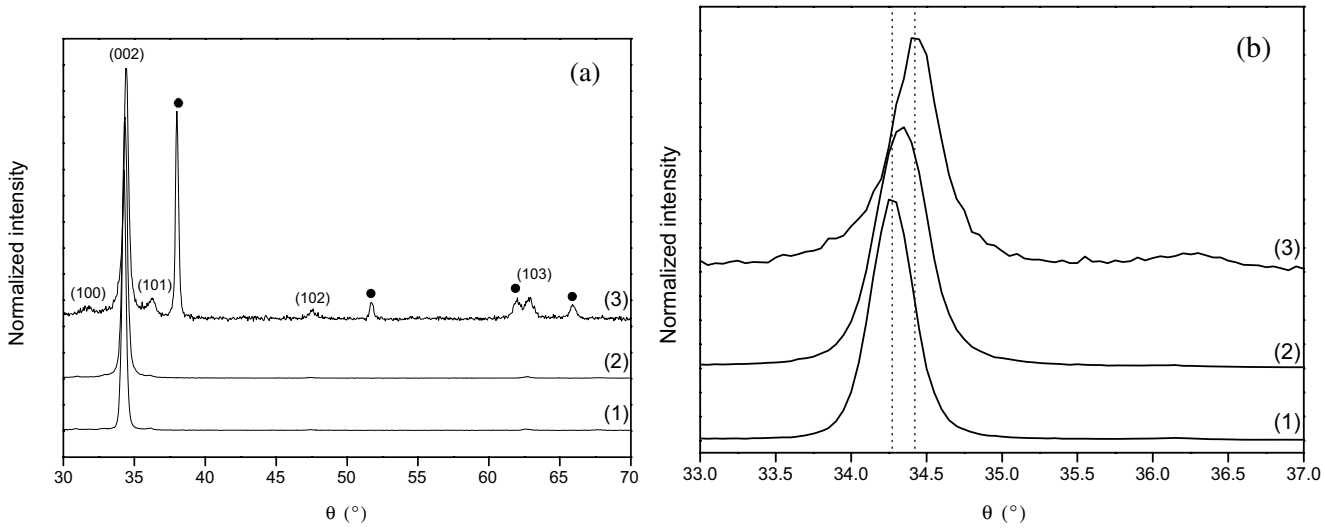

Fig. 2. (a) XRD pattern of ZnO:Al substrate (1), nanoporous ZnO electrodeposited on ZnO:Al (2) and nanoporous ZnO deposited on FTO glass (3). Dashes on (3) correspond to peaks characteristic of SnO_2. (b) Enlargement of the 002 peak area.

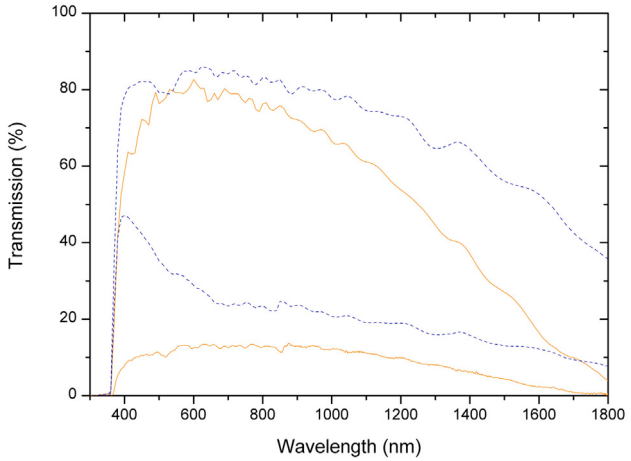

Fig. 3. Total and diffuse transmission of 5 μm thick nanoporous structure deposited on FTO glass (blue dashed line) and ZnO:Al (red full line).

incident light in the visible wavelength range. The transmission onset is very steep and corresponds to an optical band gap of 3.35 eV which is largely lower to that obtained for of an highly conductive sputtered layer (3.55 eV). These ZnO:Al layers were characterized by Hall effect and a doping level close to 5×10^{20} cm^{-3} was found. This value can also be compared to that measured for a dense ZnO layer (3.65 eV) electrodeposited in very similar experimental conditions (chloride concentration, applied potential) which contains a doping concentration up to 10^{20} cm^{-3} [36]. The shift of gap value could be related to the very high developed surface of the nanoporous ZnO that could lower the doping level of the material, but this aspect has to be investigated in more details.

The difference between the optical responses of the nanoporous morphologies described above becomes obvious when the diffuse transmission is considered. In the case of a 4 μm thick layer presented in Figure 3, the diffusive part of the transmission reaches a maximum value of 47% at 400 nm when this value is limited to 10% in the case of deposition on Al:ZnO. This effect can be related the surface roughness appearing in the case of a heterogeneous growth: the rounded elements on the top of the structure seem to strongly diffuse a part of the incident light.

3.3 Porosity and Roughness factor

Evolution of thickness and porosity of the film versus the amount of charge exchanged during electrodeposition has been studied for ZnO:ED/FTO glass and Al:ZnO/glass substrates (Fig. 4a). Porosity is calculated from the X-ray fluorescence measurements giving the amount of ZnO deposited on the substrate and the film thickness. Moreover electrochemical impedance measurements as described in Dupuy et al. [33] were performed to determine the roughness factor (Fig. 4b).

Nanoporous ZnO grows almost linearly on both substrates. Porosity of films deposited on ZnO:ED/FTO glass follows the same trend as described elsewhere [37] increasing with the thickness. For the films deposited on Al-ZnO substrate it remains constant with an average value of 55%. In all cases mechanical stability issues limit the thickness. The nanoporous structures on ZnO:ED/FTO glass could therefore be stabilized until 6 μm while deposition on ZnO:Al enables the growth until 8 μm.

Evolution of the roughness factor with the film thickness is linear for films deposited on Al:ZnO. It is not the case of films deposited on ZnO:ED/FTO glass, confirming the non homogeneous growth of these layers. Moreover, for films thicker than 6 μm, the evolution of the surface area is strongly modified and seems to be underestimated.

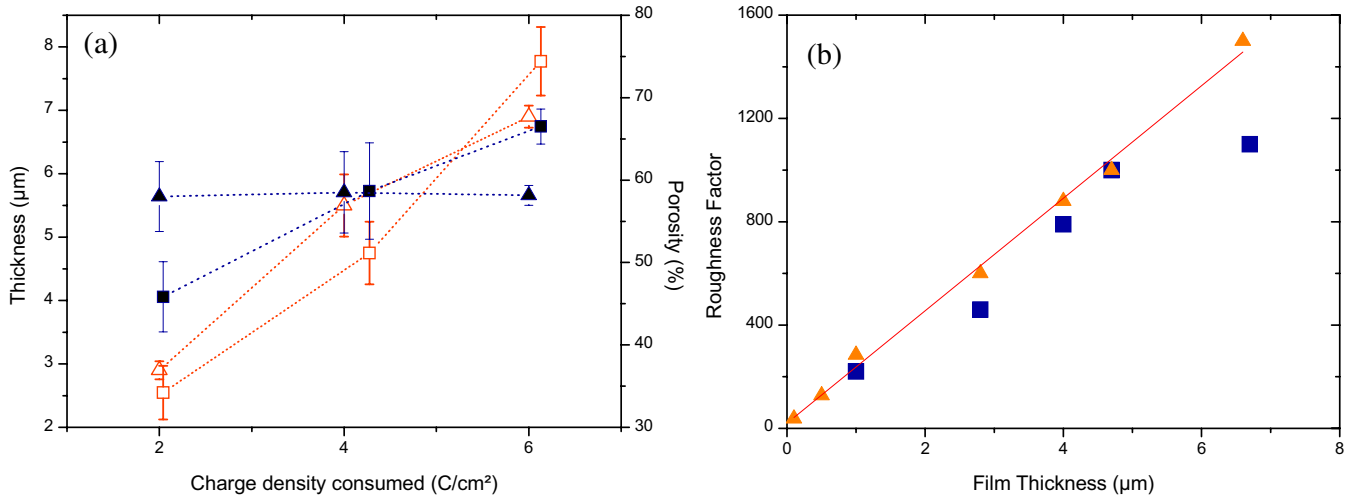

Fig. 4. (a) Evolution of film thickness (empty marks) and porosity (full symbols) of nanoporous structure deposited on FTO glass (squares) and ZnO:Al (triangles) with charge density consumed. (b) Evolution of the roughness factor of nanoporous films deposited on FTO glass (filled squares) on ZnO:Al (empty triangles) with the film thickness.

This phenomenon could be due to a partial peeling off of the layer as mentioned before. These measurements confirm the enhancement of the mechanical stability for films deposited on ZnO:Al.

Thus, a balance between the mechanical stability (presence of crack, peeling) and the thickness (related to the developed surface) has to be found for integration in DSSC.

3.4 Cell completion and photovoltaic characterization

Electrodeposited nanoporous anodes deposited on ZnO:Al were integrated into dye sensitized solar cells (N719 and D149). Different coloration durations (ranging from 30 min to 15 h at room temperature) and nanoporous ZnO thicknesses were investigated for both of the dyes.

Because of its acidic functions, N719 damages zinc oxide [38]. Thus, short coloration durations (inferior to 5 h) have been considered.

Figure 5a shows the total transmission of films of increasing thicknesses loaded with N719 at room temperature for 2 h as a function of the wavelength. Transmission of a nanoporous film free of dye molecule is given as reference. An increase of the absorption of the light is achieved by an increase of the film thickness. However, the amount of molecules loaded in the thickest films (6.6 μm) is too low to harvest all the incident light in the absorption range of N719. For 3 μm thick films, absorption occurs between 370 nm (ZnO gap) and 700 nm. An increase of the film thickness leads to a broadening of the absorption range up to 800 nm. The amount of molecules loaded on the film is calculated from the transmission data and from the molar extinction coefficient of N719 (13900 L M^{-1} cm^{-1} at 530 nm) (inset in Fig. 5a). Evolution is linear and an optimum of 100 nmol/cm^2 of N719 molecules is calculated for a 6.6 μm thick film.

Same measurements have been performed for the loading of D149 (Fig. 5b). In this case, films of thickness between 150 nm and 6.5 μm have been considered. As for sensitization with N719, an increase of the absorption is observed until 3 μm thick films. Above that limit, dye molecules harvest almost all the light. The increase of the film thickness has therefore a little influence on the light harvesting. The absorption range of the D149 is broadened by the increase of dye molecules loading and a maximum occurs at 3 μm with an absorption range between 370 nm and 650 nm. The amount of dye molecules loaded depending on the roughness surface, given in inset of Figure 5b, shows a linear evolution. A loading of 27 nmol/cm^2 could be measured for 3 μm thick films.

The higher absorption of films loaded with D149 than the ones loaded with N719 despite lower amount of dye molecules is explained by the difference of molar extinction coefficient (68700 L M^{-1} cm^{-1} at 541 nm for the D149 compared to 13900 L M^{-1} cm^{-1} at 530 nm for the N719).

Solar cells have been prepared to compare both the effect of substrate and dye on the photovoltaic characteristics. Figure 6 presents selected current voltage curves under illumination for these different conditions. Corresponding photovoltaic parameters are shown in Table 1.

Solar cells prepared from nanoporous ZnO grown on ZnO:Al covered by N719 molecules exhibit an increased Jsc and fill factor (FF) with the film thickness while the Voc remains stable (see table 1). The highest Jsc (10.1 mA/cm^2) was recorded for 6.5 μm thick films after 2 h of coloration. The maximal value for Jsc expected in regard to the ZnO:Al substrate transmission and the absorption range of N719 is ca. 18 mA/cm^2. Such Jsc values could not be obtained unless saturation occurs at every wavelength. Best efficiency (4.2%, Voc 595 mV, FF 72% see Fig. 6 and Table 1) were found to occur after 2 h of coloration with a 6.6 microns thick layer deposited on

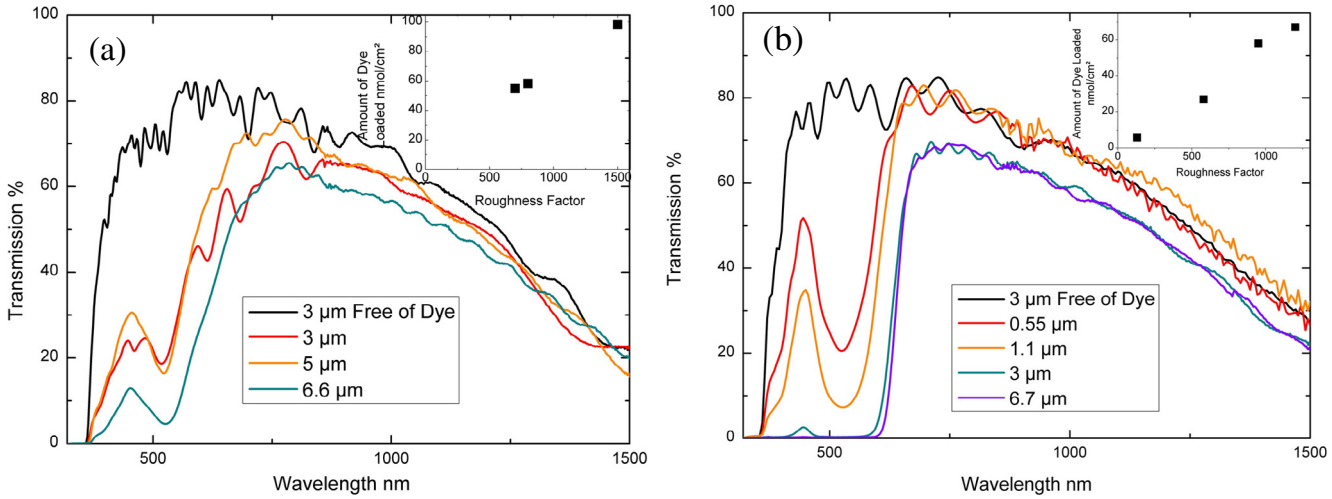

Fig. 5. Total transmission of nanoporous structures loaded during (a) 2 h with N719 and (b) 15 h with D149 for increasing charge density consumed. Total transmission of a film prepared with deposition of 4 C/cm^2 is given as reference. Insets of each figure represents the evolution of the amount of dye molecules loaded with respect to the developed surface calculated from the transmission data.

Table 1. Photovoltaic properties of dye sensitized solar cells based on ZnO electrodeposited on different substrates and for different coloration conditions.

Substrate	Dye	Coloration time	Thickness μm	Jsc mA/cm^2	Voc mV	FF	Efficiency %
FTO	N719	2h	6.5	10.4	562	65	3.8
Al:ZnO	N719	2h	3	5.5	580	68	2.2
	N719	2h	6.6	9.7	592	72	4.2
	D149	2h	3	10.1	573	71	4.2
	D149	15h	3	10.3	592	73	4.5

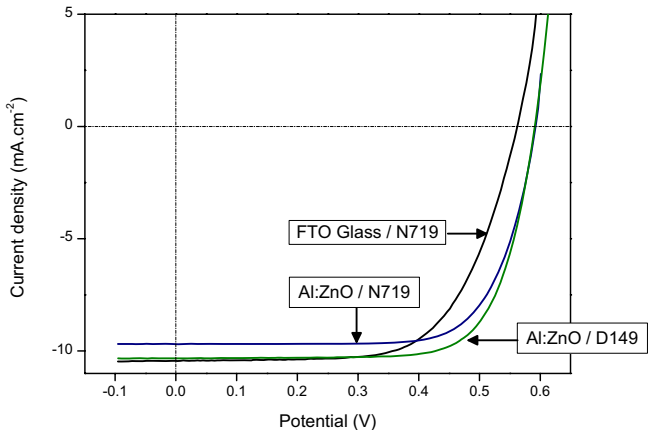

Fig. 6. Current density – voltage characteristics of dye-sensitized solar cells based on nanoporous ZnO grown on FTO glass and dyed with N719 for 2 h, on ZnO:Al and dyed with N719 for 2 h and grown on ZnO:Al and dyed with D149 for 15 h.

ZnO:Al; a thickness below the mechanical stability limit of these films.

ZnO anode grown on ZnO:ED/FTO glass in the same conditions could achieve a maximum efficiency of 3.8% (Jsc 10.4 mA/cm^2 , Voc 563 mV, FF 65%). Lower Voc and FF obtained with these films could be related to inferior transfer properties at the interface between nanoporous ZnO and the substrate and to the lower organization of the structure, leading to additional recombination paths.

No dissolving effect is reported when dipping ZnO in a D149 coloration bath but formation of dye aggregates have been observed elsewhere for long time of coloration [32].

Thus, three dipping conditions for coloration have been studied: 10 min, 2 h and 15 h. Best results were found to occur after dipping the films for 15 h.

Figure 7a shows the spectral response of films with thicknesses ranging from 1.1 μm to 4.5 μm dyed for 2 h. The wavelength range of the electron collection is broadened with the increase of the thicknesses. This is consistent with the transmission data that show an increase of the amount of dye molecules loaded. Higher concentrations of dye enhance the light harvesting at low molar extinction coefficient wavelength and electrons from a broader wavelengths range, and the corresponding energies can therefore be absorbed. At the absorption peaks of the D149 dye, electron quantum efficiency reaches a maximum for a 3 μm thick film and then decreases. Figure 7b shows that both Jsc calculated from spectral response spectra and measured with the solar simulator also reach an optimum for 3 μm thick film. Since a linear increase of the amount

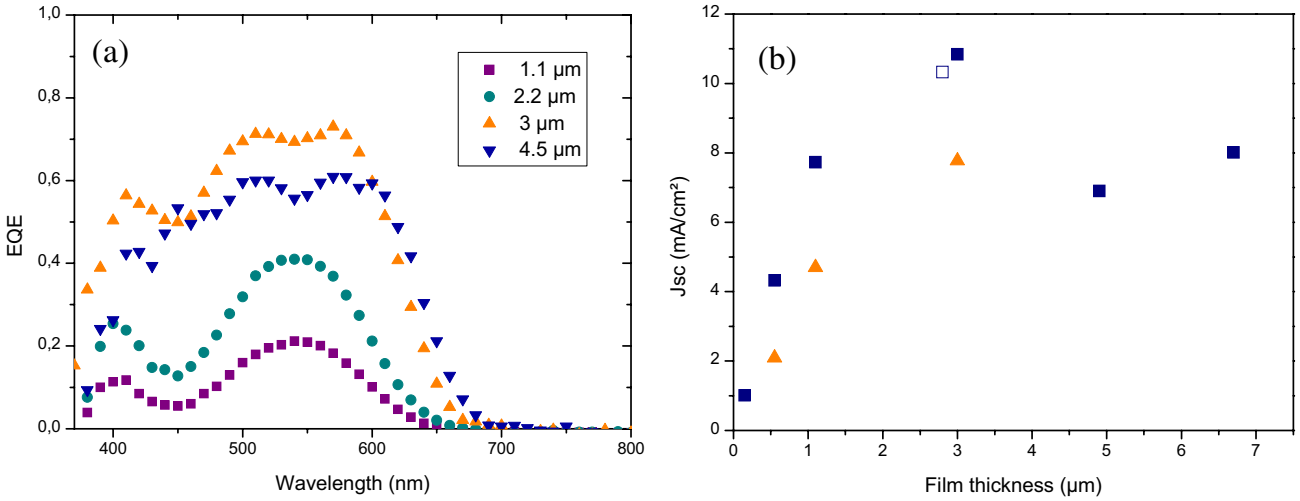

Fig. 7. (a) Spectral response of dye-sensitized solar cells based on nanoporous ZnO grown on ZnO:Al of increasing thicknesses and dyed with D149 for 2 h. (b) Evolution of the Jsc measured with the solar simulator (squares) and calculated from the spectral response (triangles) with the thickness of the nanoporous ZnO in the same coloration conditions. Jsc of the best cell is shown (empty square).

of dye molecules could be calculated from transmission data, Jsc is firstly limited by the dye concentration and, for the highest thicknesses tested, by a lowering of the injection efficiency. Same trend has been observed for each coloration condition. It is worth noting that Jsc calculated from spectral response is underestimated due to the fact that spectral responses are carried out under lower light illumination where traps are more actives.

Optimal conditions, that is to say 3 μm thick films dipped 15 h in the coloration bath, exhibit Jsc of 10.3 mA/cm^2 . Maximal Jsc calculated from ZnO:Al substrate transmission in an absorption range until 650 nm is 13 mA/cm^2 . This value shows that the structure enables to collect almost 80% of the theoretical photocurrent available. Further improvement of the transparency could allow to reach short circuit photocurrent up to 15 mA/cm^2.

Open circuit voltages are in the range of 600 mV and are slightly lower than value of 650 mV reported in the literature for D149 [39]. The same dye on TiO_2 could achieve a Voc of almost 700 mV [31]. Fill Factors are typically up to 70%. Both parameters were found to increase with the coloration.

Finally, an efficiency of 4.5% (Jsc 10.3 mA/cm^2 , Voc 592 mV, FF 73%) could be recorded for a 3 μm thick film with 15 h of coloration.

4 Conclusion

In this paper, we have shown for the first time that it is possible to deposit successfully nanoporous ZnO on sputtered Al:ZnO with a facilitated nucleation and a higher adhesion of the nanoporous structure to the substrate as a result. A highly regular and organized structure with pores in the nanorange perpendicular to the substrate could be observed. Porosity of 55% has been obtained and developed surface was shown to evolve linearly with the film thickness.

Solar cells prepared with nanoporous ZnO deposited on ZnO:Al substrate showed superior properties for Voc and FF as compared to FTO substrate in our study. Both N719 and D149 have been used to sensitize the ZnO. Efficiencies up to 4.5% and 4.2% could be obtained for sensitization with D149 and N719 respectively. Room for improvement exists, in particular with respect to the short circuit current, which could reach a level of 15 mA/cm^2 .

The authors would like to acknowledge the ANR Asyscol program for support.

References

1. B. O'Regan, M. Gratzel, Nature **353**, 737 (1991)
2. M. Gratzel, Nature **414**, 338 (2001)
3. C. Klingshirn, Phys. Stat. Sol. (b) **71**, 547 (1975)
4. C. Kormann, D.W. Bahnemann, M.R. Hoffmann, J. Phys. Chem. 5196 (1988)
5. D. Look, Mat. Sci. Eng. B **80**, 383 (2001)
6. G. Boschloo, T. Edvinsson, A. Hagfeldt, in: Nanostructured Materials for Solar Energy Conversion, edited by Elsevier, (2006: p. 227)
7. E. Hosono, Y. Mitsui, H. Zhou, Dalton Transactions 5439 (2008)
8. A. Umar, A. Al-Hajry, Y. Hahn, D. Kim, Electrochim Acta **54**, 5358 (2009)

9. C.Y. Jiang, X.W. Sun, G.Q. Lo, D.L. Kwong, J.X. Wang, Appl. Phys. Lett. **90**, 263501 (2007)
10. W. Chen, H. Zhang, I.M. Hsing, S. Yang, , Electrochem. Commun. **11**, 1057 (2009)
11. A.R. Rao, V. Dutta, Nanotechnology 445712 (2008)
12. S. Peulon, D. Lincot, Adv. Mater. **8**, 166 (1996)
13. M. Izaki, T. Omi, Appl. Phys. Lett. **68**, 2439 (1996)
14. T. Yoshida, H. Minoura, Adv. Mater. **12**, 1219 (2000)
15. J. Elias, R. Tena-Zaera, C. Lévy-Clément, J. Electroanal. Chem. **621**, 171 (2008)
16. J. Elias, R. Tena-Zaera, G. Wang, C. Lévy-Clément, Chem. Mat. **20**, 6633 (2008)
17. K. Kakiuchi, M. Saito, S. Fujihara, Thin Solid Films **516**, 2026 (2008)
18. Y.Y. Xi, Y.F. Hsu, A.B. Djurisic, W.K. Chan, J. Electrochem. Soc. **155**, D595 (2008)
19. S. Haller, T. Suguira, D. Lincot, T. Yoshida, Phys. Stat. Sol. (a) **207**, 2252 (2010)
20. Z. Chen, Y. Tang, L. Zhang, L. Luo, Electrochim. Acta **51**, 5870 (2006)
21. Q. Zhang, C.S. Dandeneau, X. Zhou, G. Cao, Adv. Mater. **21**, 4087 (2009)
22. T. Yoshida, J. Zhang, D. Komatsu, S. Sawatani, H. Minoura, T. Pauporté, et al., Adv. Funct. Mater. **19**, 17 (2009)
23. H. Minoura, T. Yoshida, Electrochemistry 109 (2008)
24. V.M. Guerin, C. Magne, T. Pauporte, T. Le Bahers, J. Rathousky, ACS Appl. Mater. Interfaces **2** 3677 (2010)
25. T. Pauporte, D. Lincot, Appl. Phys. Lett. **75** 3817 (1999)
26. T. Loewenstein, M. Rudolph, M. Mingebach, K. Strauch, Y. Zimmermann, Yvonne), A. Neudeck, Andreas, S. Sensfuss, D. Schlettwein, Chem. Phys. Chem. **11**, 783 (2010)
27. T. Loewenstein, J. Sann, C. Neumann, B. K. Meyer, D. Schlettwein, Phys. Stat. Sol. (a) **10**, 2382 (2008)
28. K. Keis, E. Magnusson, H. Lindström, S. Lindquist, A. Hagfeldt, Sol. Energy Mat. Sol. Cells **73**, 51 (2002)
29. T. Horiuchi, H. Miura, K. Sumioka, S. Uchida, J. Am. Chem. Soc. **126**, 12218 (2004)
30. M. Grätzel, Comptes Rendus Chimie. **9**, 578 (2006)
31. M. Matsui, A. Ito, M. Kotani, Y. Kubota, K. Funabiki, J. Jin, et al., Dyes and Pigments **80**, 233 (2009)
32. Y. Sakuragi, X. Wang, H. Miura, M. Matsui, T. Yoshida, J. Photochem. Photobiol. A: Chemistry **216**, 1 (2010)
33. L. Dupuy, S. Haller, J. Rousset, F. Donsanti, J. Guillemoles, D. Lincot, et al., Electrochem. Commun. **12**, 697 (2010)
34. T. Yoshida, T. Pauporte, D. Lincot, T. Oekermann, H. Minoura, J. Electrochem. Soci. **150**, C608 (2003)
35. Z. Jehl, J. Rousset, Nanotechnology 395603 (2010)
36. J. Rousset, E. Saucedo, D. Lincot, Chem. Mat. **21**, 534 (2009)
37. B.R. Sankapal, J. Zhang, T. Yoshida, H. Minoura, Trans. Mat. Res. Soci. Japan 429 (2006)
38. H. Horiuchi, R. Katoh, K. Hara, M. Yanagida, S. Murata, H. Arakawa, M. Tachiya, J. Phys. Chem. B **107**, 2570 (2003)
39. H. Cheng, W. Hsieh, Nanotechnology 485202 (2010)